Received: 22 May 2023 | Revised: 21 August 2023 | Accepted: 7 September 2023

DOI: 10.1002/prep.202300139

Propellants, Explosives, Pyrotechnics

RESEARCH ARTICLE

Analysis of the thermal decomposition of munitions wastewater

Roshan Adhikari[1] | **Nick Parziale**[1] | **Tsan-Liang Su**[2] | **Washington Braida**[2] | **Christos Christodoulatos**[2]

[1]Department of Mechanical Engineering, Stevens Institute of Technology, Hoboken, US

[2]Department of Civil, Environmental and Ocean Engineering, Stevens Institute of Technology, Hoboken, US

Correspondence
Nick Parziale, Department of Mechanical Engineering, Stevens Institute of Technology, Hoboken, NJ, 07030, US.
Email: nick.parziale@gmail.com

Abstract

The thermal decomposition of ammonium nitrate (AN) laden munitions wastewater and comparable control samples were studied under air and nitrogen environments at pressures from 0.1 MPa to 10 MPa. The decomposition enthalpies, measured using a Differential Scanning Calorimeter (DSC), and gaseous emissions, measured using a Fourier-Transform Infrared Spectrometer (FTIR), were used to evaluate the quality of decomposition. Experiments demonstrated that higher pressures improved the energy yield and reduced the quantities of harmful NO_x from the decomposition of all samples. At 10 MPa, experimentally measured decomposition enthalpy from the munitions wastewater was 1.8 MJ/kg, approximately 45% of its standard enthalpy of decomposition, and NO and NO_2 accounted for only 0.7% and 0.08% of the nitrogen in the sample, respectively. The emissions stream from the wastewater was found to primarily consist of N_2, CO_2, H_2O and N_2O. An analysis of the heat releases and the emissions showed that higher pressures improved the extent and enthalpy of decomposition by preventing premature loss of gaseous intermediates and sensible heat through the pin-hole crucibles used in the experiments. Moreover, high pressures precluded the evaporation of water and promoted the decomposition of AN via a radical mechanism.

KEYWORDS
ammonium nitrate, emissions analysis, munitions wastewater, thermal analysis, thermal decomposition

1 | INTRODUCTION

Ammonium Nitrate (AN) is the nitrate salt of ammonium and one of the most widely used ammonium compounds [1]. It is used in fertilizers, and propellants, and is the primary component of many industrial explosives [1–3]. AN has a positive oxygen balance of +20%, and therefore is often used as the oxidizing compound in many types of explosives [4]. This work focuses on the AN-laden wastewater from the fabrication of energetic materials in an industrial munitions plant. This wastewater is called AN Solution or "ANSol", and contains AN, water, methylammonium nitrate (MAN), dimethylammonium nitrate (DMAN), trimethylammonium nitrate (TMAN), and nitramine explosives (RDX and HMX). The exact proportions of the various species in the wastewater vary according to upstream products and processes.

Because of its composition, the ANSol wastewater must be disposed of in accordance with regulatory guidelines. However, the presence of oxygen-rich AN and carbon-containing alkylamine nitrates and explosives results in the opportunity that the ANSol wastewater could be repurposed as a monofuel for energy harvest.

Therefore, thermal decomposition of the ANSol wastewater could be an attractive alternative to current costly and energy-intensive disposal methods. For this approach to be beneficial, the energy release should be maximized and the NO_x emissions should be minimized. To this end, an ANSol treatment parameter space is explored where temperature and pressure are varied within potential large-scale reactor values.

In this work, the feasibility of converting the wastewater to an energy source is evaluated by measuring the energy release from the decomposition of the munitions wastewater and control samples of comparable compositions. Additionally, gaseous emissions from the decomposition of all samples are analyzed to assess the environmental impact of such decomposition. The major decomposition mechanisms of the samples are discussed within the context of existing literature. This study showed that higher pressures improved the extent and enthalpy of decomposition by reducing the loss of gaseous intermediates from the DSC crucibles. At a high pressure (10 MPa), the wastewater had an observed decomposition enthalpy of 1.8 MJ/kg, and NO and NO_2 accounted for only 0.7% and 0.08% of the nitrogen in the sample respectively.

2 | REVIEW OF AN DECOMPOSITION MECHANISMS

The thermal decomposition of the munitions wastewater is dictated by the thermolysis of AN since it is the primary component of the wastewater. Therefore, AN decomposition mechanisms are relevant to this work, and the AN decomposition literature is discussed in this section. As an onium salt, AN is known to dissociate into its acid and base molecules per reaction 1 shortly after its melting point of 170 °C [2, 3].

$$NH_4NO_3 \rightarrow NH_3 + HNO_3 \quad (1)$$

AN is also known to undergo exothermic decomposition to N_2O and H_2O per reaction 2 [1, 2, 5–7].

$$NH_4NO_3 \rightarrow N_2O + 2H_2O \quad (2)$$

Rosser et al. [8] suggested that AN dissociation and decomposition (reactions 1 and 2) are coupled. The exothermic decomposition of AN is facilitated by the reaction of NH_3 with the oxidizing species produced from the decomposition of HNO_3. The reaction pathway of HNO_3 decomposition is dependent on the temperature; an ionic dissociation (reaction 3) is dominant immediately after melting of AN at 170 °C [8], but a radical decomposition (reaction 6) becomes the dominant mechanism after 290 °C [9]. Consequently, decomposition of AN follows two different pathways depending on the temperature as shown in Scheme 1 and Scheme 2 below.

Scheme 1*: Ionic decomposition* [8]:

$$2HNO_3 \leftrightarrow NO_2^+ + NO_3^- + H_2O \quad (3)$$

$$NH_3 + NO_2^+ \rightarrow N_2O + H_3O^+ \quad (4)$$

$$H_3O^+ + NO_3^- \leftrightarrow HNO_3 + H_2O \quad (5)$$

Scheme 2*: Radical decomposition* [9]:

$$HNO_3 \overset{slow}{\rightarrow} HO^\bullet + NO_2^\bullet \quad (6)$$

$$HO^\bullet + NH_3 \rightarrow H_2O + NH_2^\bullet \quad (7)$$

$$NH_2^\bullet + NO_2^\bullet \rightarrow NH_2NO_2 \quad (8)$$

$$NH_2NO_2 \rightarrow N_2O + H_2O \quad (9)$$

Schemes 1 and 2 represent the most widely proposed mechanisms for AN decomposition [1]. However, the exact mechanism depends on various factors such as pressure, temperature, and the type of additives, if any. Therefore, multiple other reaction pathways have been proposed, a comprehensive compilation of which is available in a recent review by Babrauskas and Leggett [10].

The decomposition of AN mixtures is significantly affected by the type of additives in the mixture. The effect of carbon-based additives is particularly relevant to this work due to the presence of carbonaceous species in the ANSol wastewater. Sinditskii et al. [3] found that many organic substances promote AN burning in a weak manner, while charcoal, wood flour, and soot enhance AN decomposition significantly. Similarly, Izato et al. [7] determined that the physical nature of the carbon additive, and whether it is activated has a significant impact on AN decomposition, and reported that HNO_3 from AN dissociation acts as an oxidizer for the combustion of the sample carbon. Lurie and Lianshen [11] reported that the presence of carbon black increased the decomposition rate of solid AN by more than seven orders of magnitude. In another study, Xu et al. [12] reported that inorganic carbon is almost non-reactive with AN,

but organic carbon acts as a catalyst in AN dissociation.

3 | EXPERIMENTAL

3.1 | Materials

The ANSol wastewater investigated in this study is named "Final Sludge" (FS) wastewater, and was obtained from an industrial munitions plant. It consists of AN, MAN, DMAN, TMAN, water, and explosives. Additionally, two control samples were prepared with AN, MAN, and water. In the first control sample, named "Control 1" (C1), the ratio of AN to MAN was equal to the ratio of AN to MAN, DMAN, TMAN, and explosives in the FS sample. In the second control sample, named "Control Stoichiometric" (CS), AN and MAN were mixed in stoichiometric proportions as determined from reaction 10. Water was added to both control samples for ease of handling. The species compositions of all samples by mass percentages of their constituent species are shown in Table 1, and the elemental compositions of all samples by mass percentages of their constituent elements are shown in Table 2.

The MAN used in the control samples was obtained by neutralization of methylamine (MA) solution (40 wt% in H_2O) and nitric acid (HNO_3, 0.1 M), both from Sigma Aldrich. The HNO_3 was diluted with DI water prior to the neutralization reaction. The quality of the synthesized MAN was determined to be sufficient by comparing its DSC thermogram with the one reported by Parker [13].

3.2 | Equipment

The experimental setup is shown in Figure 1. Thermal analyses of samples were performed in a Mettler Toledo High Pressure Differential Scanning Calorimeter (HP DSC 2+). The flow of the purge gas to the DSC was controlled by a Brooks SLA5850 mass-flow controller installed upstream of the DSC. Additionally, there was a Brooks SLA5820 pressure controller installed downstream of the DSC.

Evolved gases were measured using a Nicolet is50 Fourier-Transform Infrared (FTIR) Spectrometer from

TABLE 1 Species composition of the final sludge and control samples by mass percentages.

	Samples		
Species (%)	**C1**	**CS**	**FS**
AN	59	50	65
MAN	21	29	18
Water	20	21	12
DMAN			1
TMAN			1
Explosives			3

TABLE 2 Elemental composition of the final sludge and control samples by mass percentages.

	Samples		
Elements (%)	**C1**	**CS**	**FS**
C	2.7	3.7	3.4
H	6.5	6.7	6.1
N	26.8	26.1	29.4
O	64.0	63.5	61.1

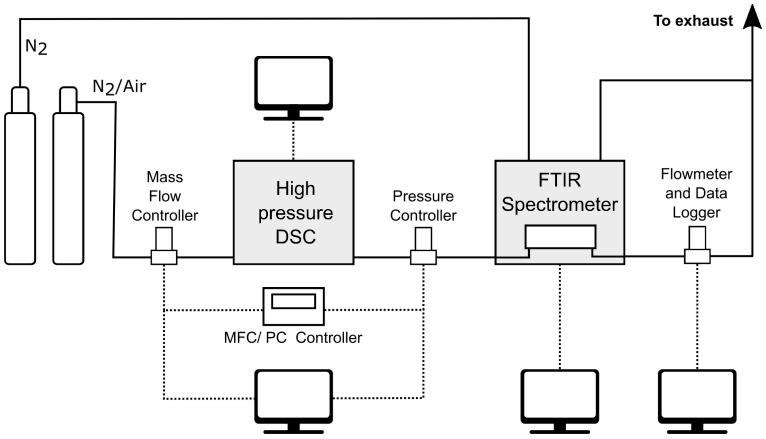

FIGURE 1 Experimental setup for thermal and emissions analysis.

ThermoFisher Scientific. The spectrometer was equipped with a gas cell of 10 cm pathlength with silver bromide (AgBr) windows. A Deuterated Triglycine Sulfate (DTGS) detector was used to collect spectra of the emissions between 1000 and 4000 cm^{-1} with a resolution of 8 cm^{-1}. An optical velocity of 0.6329 was used for the DTGS detector, and 14 scans were averaged to record one spectrum every 7.34 seconds. Atmospheric pressure and room temperature (22 °C) were maintained inside the gas cell during data collection. The FTIR was calibrated for five gases, namely carbon monoxide (CO), carbon dioxide (CO_2), nitric oxide (NO), nitrogen dioxide (NO_2) and nitrous oxide (N_2O), using calibration standards of primary master grade from Linde Gas and Equipment (formerly Praxair Inc). An Aalborg XFM gas flowmeter and data logger downstream of the FTIR was used to measure the gas flow rates.

3.3 | Methods

Sample containers were submerged in a water bath maintained at 80 °C for two hours prior to sample preparation to prevent AN precipitation and obtain a homogeneous solution. Samples of up to 5 mg were used for the low-pressure experiments, and samples of up to 10 mg were used for the high-pressure experiments. Larger samples were used at higher pressures so that minor species could be detected more easily. Experiments were performed in standard 40 μl aluminum crucible with lids perforated with a hole of about 0.5 mm. Prior to starting each experiment, the CO_2 concentration was monitored while the DSC, FTIR, and gas cell were purged with research-grade nitrogen. Experiments were performed after the measured CO_2 concentration attained a stable value near zero and a new FTIR background was obtained. The sample was then heated from 40 °C to 400 °C at 20 °C/min, and the DSC was held at 400 °C to prevent pressure drop and maintain the purge of the evolved gases into the FTIR. The flow rate into the DSC was set to 200 mL/min. This higher-than-typical flow rate was used to speed up the purging of the gaseous emissions produced from the samples.

4 | RESULTS AND DISCUSSION

To establish benchmarks with which to compare the experimental data, the thermal decomposition of the wastewater is idealized via stoichiometric reactions of AN with the methylammonium nitrates (MANs) (reactions 10 through 12), and with RDX and HMX (reactions 13 and 14 respectively). The thermal decomposition of the control samples are idealized via the reaction between AN and MAN (reaction 10). The excess AN in the C1 and FS samples is assumed to decompose to N_2O and H_2O per per reaction 2.

Ideal reactions of AN with MANs and explosives:

$$[CH_3NH_3]NO_3\,(aq) + 2\,NH_4NO_3\,(aq) \rightarrow CO_2\,(g) + 3\,N_2\,(g) + 7\,H_2O\,(l), \quad \Delta H^o_{rxn} = -1.4\,MJ \tag{10}$$

$$[(CH_3)_2NH_2]NO_3\,(aq) + 5\,NH_4NO_3\,(aq) \rightarrow 2\,CO_2\,(g) + 6\,N_2\,(g) + 14\,H_2O\,(l), \quad \Delta H^o_{rxn} = -2.8\,MJ \tag{11}$$

$$[(CH_3)_3NH]NO_3\,(aq) + 8\,NH_4NO_3\,(aq) \rightarrow 3\,CO_2\,(g) + 9\,N_2\,(g) + 21\,H_2O\,(l), \quad \Delta H^o_{rxn} = -4.2\,MJ \tag{12}$$

$$C_3H_6N_6O_6\,(s) + 3\,NH_4NO_3\,(aq) \rightarrow 3\,CO_2\,(g) + 6\,N_2\,(g) + 9\,H_2O\,(l), \quad \Delta H^o_{rxn} = -2.8\,MJ \tag{13}$$

$$C_4H_8N_8O_8\,(s) + 4\,NH_4NO_3\,(aq) \rightarrow 4\,CO_2\,(g) + 8\,N_2\,(g) + 12\,H_2O\,(l), \quad \Delta H^o_{rxn} = -3.7\,MJ \tag{14}$$

Reactions 10 through 14 represent an idealized case with stoichiometric reactions producing only N_2, CO_2 and H_2O. In the case of incomplete reactions, NO_x species are also produced [5]. The work on the thermal decomposition of a comparable urea and AN (UAN) fuel by Dana et al. [5, 14–16] and Mosevitzky et al. [17] elucidate the importance of high pressures on minimizing the amounts of harmful NO_x.

The standard enthalpies of decomposition of the samples, calculated on a per-mass basis, were assumed to represent the maximum energy release from the samples. From the sample compositions and the governing ideal reactions, these values for the C1, CS and FS samples were found to be 3.6 MJ/kg, 4.3 MJ/kg, and 4.1 MJ/kg, respectively.

Experimental decomposition enthalpies from the samples were obtained by integration of the exothermic peak(s) in their thermograms using the STARe software from Mettler Toledo. An example of such integration in a thermogram of the FS sample at 10 MPa with nitrogen purge is shown in Figure 2.

Figure 3 shows the experimentally measured decomposition enthalpies of all samples at different pressures with both N_2 and air purges, as both absolute values and as percentages of the energy content of the samples. Each bar shows the average enthalpy from multiple experiments for a set of sample composition, pressure and purge gas; the error bars show the standard deviation between individual measurements.

The energy released from all samples increase with pressure, and when using air instead of nitrogen. A sharp increase in the measured enthalpy is observed when the pressure is increased from 0.1 to 0.5 MPa, irrespective of the sample and the purge gas. Thereafter, the energy yield increases steadily with pressure. However, the decomposition enthalpies are similar at 5 and 10 MPa, except for the C1 sample with nitrogen purge. Under the inert nitrogen environment, the maximum average enthalpies from the C1, CS, and FS samples are 1.7 MJ/kg, 1.9 MJ/kg, and 1.8 MJ/kg, respectively. These measured energy releases correspond to 47%, 44%, and 44% of the calculated upper bounds for energy release (standard enthalpy of decomposition). With air purge, the maximum average enthalpies from the C1, CS, and FS samples are 1.8 MJ/kg, 2.3 MJ/kg, and 2.0 MJ/kg respectively, corresponding to 52%, 53%, and 49% of the upper bounds.

The increase in the decomposition enthalpies when using air can be attributed to the combustion of the sample carbon in the presence of oxygen in the air. However, each sample has either stoichiometric or excess of stoichiometric oxygen content – these observations therefore indicate the loss of oxidizing species from the crucible. This could include loss of AN via sublimation [18], or via recombination of NH_3 and HNO_3 in the gas phase [19]. Other possible pathways include loss of HNO_3, or its dissociation or decomposition products (reactions 3 and 6).

In the same manner, the loss of carbon and hydrogen-containing "fuel" species from the crucible is also possible. The MANs present in all samples have been known to produce volatile species such as CH_3, CH_4, CH_3NO_2 [20–22]. However, these species were not detected in the emissions stream in this work. In addition, Jain et al. [20] also found evidence of carbon particulates in the emission stream from the thermal decomposition of all MANs. Accumulation of carbon on DSC sensors when working with organic material has also been reported in literature [23]. The experiments performed in this work revealed some evidence of carbon being deposited on the crucible and along the flow lines. However, quantifying this phenomena is not possible with the current setup and may lead to undercounting carbon when performing mass balances, as will be discussed later.

The positive effect of higher pressures on measured decomposition enthalpies observed in Figure 3 is in part due to retention of volatiles and gaseous intermediates

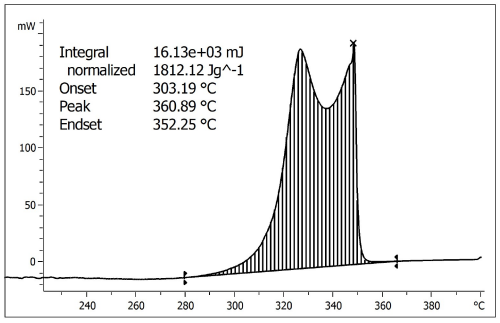

FIGURE 2 Determination of the decomposition enthalpy of the FS sample at 10 MPa with nitrogen purge by integration of its exothermic peak of decomposition.

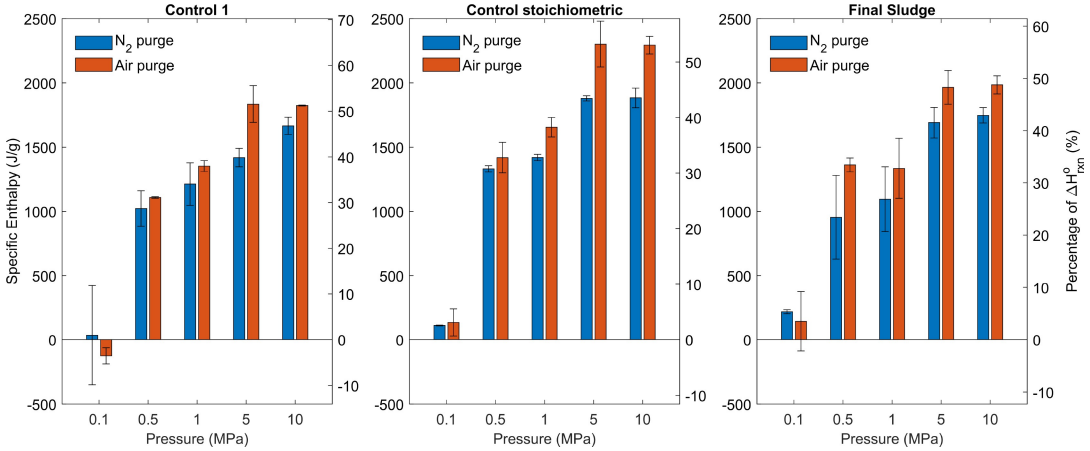

FIGURE 3 Decomposition enthalpies from the final sludge and control samples at various pressures with air and nitrogen purge. Higher pressures improve the energy yield from the samples by limiting loss of gaseous intermediates and sensible heat.

inside the pin-hole crucibles for longer time. Under high pressures, these species undergo exothermic reactions in the reaction zone of the crucible and the extent of thermal decomposition is enhanced [5, 14]. By retaining hot gaseous intermediates and products inside the crucible for longer time, higher pressures also contribute to increased heat-transfer to the DSC sensor, and limit the loss of sensible heat. Similar discussions regarding the loss of sensible heat with gaseous products and volatiles are provided in literature [24, 25].

The loss of sensible heat partly explains why measured decomposition enthalpies from all samples are smaller than the energy contents (standard enthalpies of decomposition) of those samples. For example, the maximum energy yield relative to the energy content is 53.2%, from the Control Stoichiometric sample (Figure 3). This shows that measured decomposition enthalpies do not necessarily reflect the extent of decomposition. However, since a complete decomposition of the samples would yield primarily CO_2, N_2, H_2O (and a small amount of N_2O due to non-stoichiometry), the extent of decomposition can be more reliably assessed by analysis of the gaseous emissions.

Due to their compositions, the emissions stream from the decomposition of the final sludge and the control samples include gaseous nitrogen, and oxides of carbon and nitrogen. Species analyzed in this work include CO, CO_2, NO, NO_2 and N_2O. N_2 is a primary product from all samples, but it cannot be detected by the FTIR and has to be calculated from mass balance of the nitrogen in the sample and the emissions. Similarly, while water vapor is also a major species in the emissions, it was not measured in this work. No other gaseous species were detected.

Figure 4 shows a 3D series consisting of multiple infrared absorbance spectra of evolved gases from the thermal decomposition of the FS sample at 0.5 MPa with nitrogen purge. A representative spectrum from this 3D series is also shown, and the absorption peaks of the analyzed gaseous species are identified. Figure 4 also shows the concentration profiles of the measured species from all samples at a representative pressure of 0.5 MPa with nitrogen purge against the DSC temperature and the time elapsed. For the control samples, N_2O is detected first while for the final sludge, both N_2O and CO_2 are detected simultaneously ahead of the other species. While the decomposition of each sample is complete before 350 °C at this pressure (Figure 8), the flow of evolved gases into the FTIR is delayed due to a large amount of gas inside the DSC. The concentration profiles in Figure 4, therefore, do not represent the real-time gas evolution from the samples. Another consequence of this

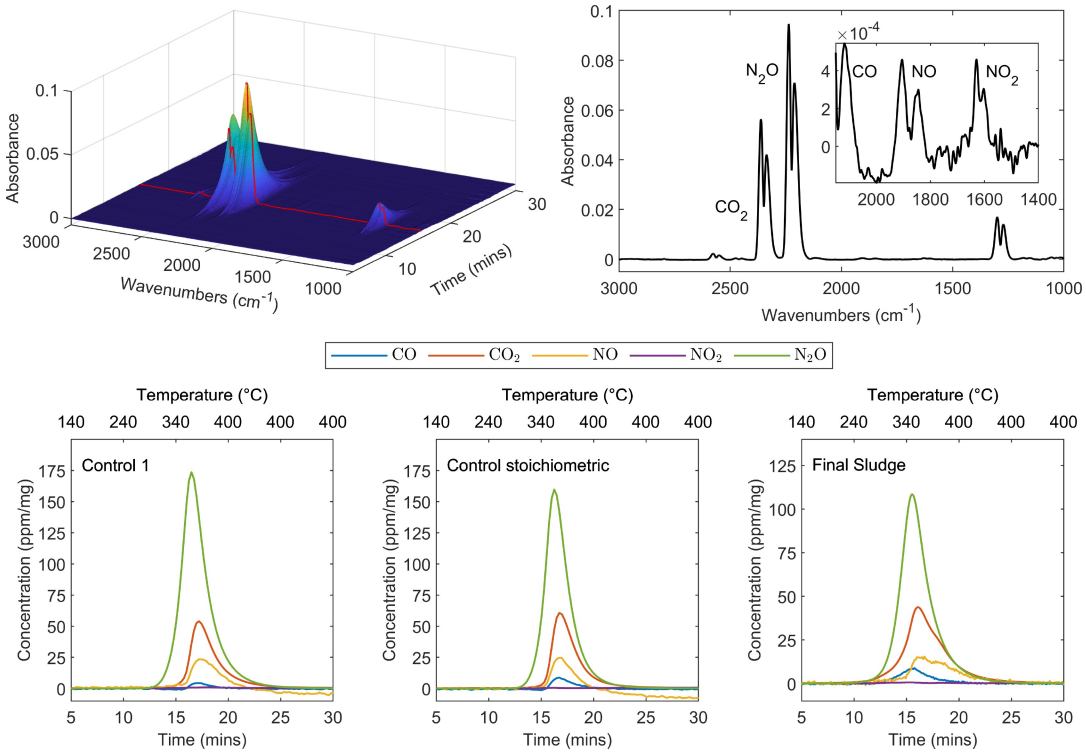

FIGURE 4 (Top left) 3D series of infrared absorption spectra of evolved gases from FS decomposition under 0.5 MPa nitrogen pressure, with a representative spectrum highlighted in red; (top right) the representative spectrum showing the absorption peaks of CO_2 and N_2O, and of CO, NO and NO_2 in the inset; (bottom) the sample-mass specific concentration profiles of evolved gases from the decomposition of C1, CS and FS samples at 0.5 MPa with nitrogen purge.

delay is that these profiles do not reflect the two-stage decomposition of the FS samples observed in Figure 8.

Due to these limitations, emissions analysis in this work is limited to discussions on the total quantities of the evolved gaseous species. These quantities were obtained from numerical integration of the temporal flow-rate profiles of the evolved gases, which were obtained by combining the concentration profiles from the FTIR (Figure 4) and the instantaneous flow rates measured by the flowmeter and data logger shown in Figure 1. The accuracy of this quantification technique was evaluated by employing the method shown in Figure 5. Standard gases of known concentrations mixed with the carrier gas (nitrogen) were measured with the FTIR spectrometer. The total amounts of the standard gases that passed through the spectrometer were obtained by combining their concentrations, flow rates, and flow durations, and also from integration of the flow-rate profiles obtained from the FTIR measurements. Quantities of standard gases obtained from these two approaches were compared, and values from FTIR measurements were found to be accurate to within ±10%.

Total quantities of measured gases, which include oxides of carbon and nitrogen, can be used to compare the

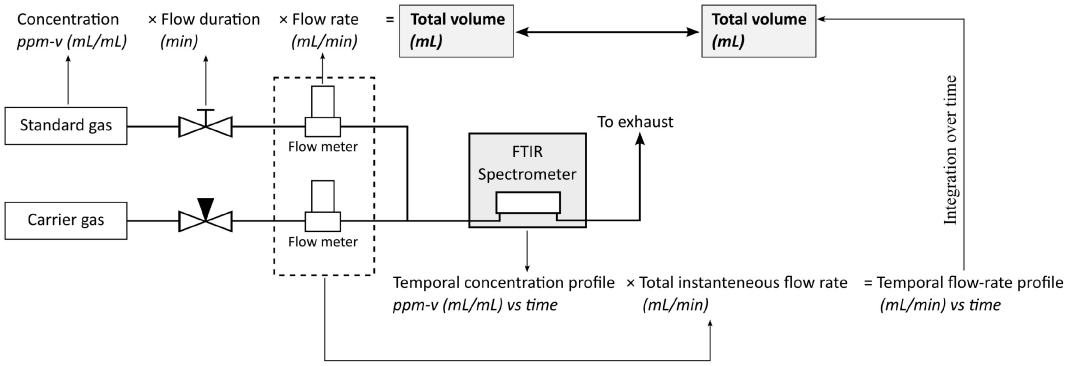

FIGURE 5 Representation of the technique used to evaluate the accuracy of gaseous emissions quantification from FTIR measurements.

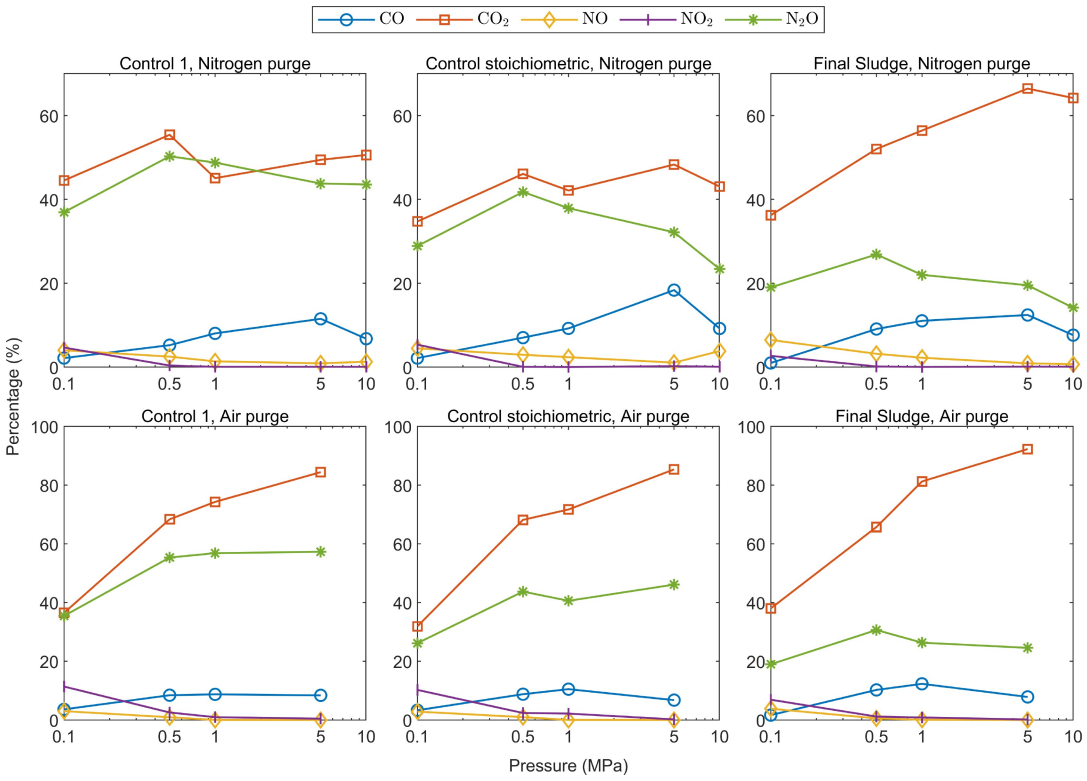

FIGURE 6 Mass percentages of sample carbon and nitrogen in gaseous emissions (CO and CO_2 for carbon, and NO, NO_2 and N_2O for nitrogen).

amounts of carbon and nitrogen in their oxides with their amounts in the sample. The mass percentages of the sample carbon and nitrogen in their respective oxides in the emissions stream are shown in Figure 6. A 45% value for CO_2 (Control 1 with nitrogen purge at 0.1 MPa) means that 45% of the sample carbon was oxidized to CO_2. The results from 10 MPa experiments with air purge are omitted in Figure 6 due to erroneous observed values of CO and CO_2 which were the result of combustion of carbon particulates from the samples deposited along the flow lines in the DSC on prior experiments. This issue did not impact other experiments.

In Figure 6, the amount of CO_2 is higher than the amount of CO for all samples with both nitrogen and air purge. With nitrogen purge, the CO_2 yield from FS sample increases with pressure, and about 67% of the carbon in the FS sample is oxidized to CO_2 at 5 MPa. No such trend is apparent in the CO_2 yield from the control samples. At pressures of 1 MPa and higher, around 40 to 50% of the sample carbon in the control samples is oxidized to CO_2. However, for all samples, the amount of CO first increases with pressure up to 5 MPa and decreases when pressure is increased further to 10 MPa. When using air as the pressurizing and purge gas, the amount of CO decreases for all samples suggesting its oxidation to CO_2. On the other hand, the amount of CO_2 increases significantly when using air compared to when using nitrogen.

N_2O is the primary nitrogen oxide detected in all experiments. The amount of N_2O increases significantly when pressure is increased from 0.1 MPa to 0.5 MPa. This increase in N_2O is accompanied by a corresponding decrease in the amounts of NO and NO_2. The mass fraction of nitrogen oxides tends to decrease with pressure after 0.5 MPa. For the FS sample with nitrogen purge at 0.1 MPa, NO, NO_2 and N_2O respectively account for 6.5%, 2.7% and 19% of the sample nitrogen, whereas at 10 MPa, they account for 0.64%, 0.08% and 14.1% of the sample nitrogen. By applying mass balance, gaseous N_2 accounts for 72% and 85% of the mass of nitrogen in the FS sample at 0.1 MPa and 10 MPa, respectively. This observation highlights the importance of high pressures in reducing the amounts of NO_x and increasing the amount of gaseous N_2. A similar observation regarding the pressure effect on the amounts of N_2 and NO_x from an aqueous urea and ammonium nitrate mixture is described by Dana et al. [15].

With air purge, the amounts of NO and NO_2 decrease with increasing pressure, but the amount of N_2O remains fairly stable above 0.5 MPa. Additionally, relative to N_2 purge, the amounts of NO_2 and N_2O increase, and that of NO decreases in an air environment. These observations highlight the role of NO_2 in oxidizing the carbon in the sample according to reaction 15 [26, 27].

$$2NO_2 + C \rightarrow CO_2 + 2NO \tag{15}$$

Under an air environment, the excess oxygen can react with sample carbon to produce CO and CO_2 according to reactions 16 and 17. This inhibits reaction 15, and leads to larger amounts of NO_2 and smaller amounts of NO. Furthermore, since NO_2 contributes to N_2O formation according to reactions 8 and 9, inhibition of reaction 15 would also lead to larger amounts of N_2O in the emissions. Observed effects of air purge on the quantities of NO, NO_2 and N_2O are therefore consistent with inhibition of redox reactions between NO_2 and sample carbon.

$$C + \frac{1}{2}O_2 \rightarrow CO \tag{16}$$

$$C + O_2 \rightarrow CO_2 \tag{17}$$

The N_2 and CO_2 masses from experimental measurements are compared to theoretical yields to evaluate the extent of decomposition. A complete decomposition of the samples would yield CO_2, N_2 and H_2O by reactions of AN with MANs and explosives (reactions 10 to 14), and H_2O and N_2O from decomposition of AN (reaction 2). Figure 7 shows the mass fractions of the sample carbon oxidized to CO_2 and the mass fractions of sample nitrogen liberated as gaseous N_2 from all experiments. The dotted lines show the theoretical limit of N_2 for each sample; the theoretical limit of CO_2 is 100% for all samples. Results from 10 MPa experiments with air purge are omitted, as was the case in Figure 6.

Gaseous N_2 and CO_2 yields are higher from the final sludge samples than from the control samples. The N_2 yield from the FS sample at 10 MPa with nitrogen purge is almost 100% of the theoretical limit, but the CO_2 yield only about 64%, and the total amount of carbon oxidized to CO and CO_2 is about 72% (Figure 6). This suggests the decomposition of nitrogen oxides to N_2 and O_2 without reacting with the carbon in the sample.

Analysis of gaseous emissions (Figure 6 and Figure 7) show that higher pressures enhance the decomposition extent of the final sludge sample. The effect of higher pressures on the extent of decomposition of the control samples is comparatively weaker. With a nitrogen purge, the N_2 and CO_2 yields from the control samples are comparable at all pressures. However, the measured decomposition enthalpies at 0.1 MPa are much lower than at higher pressures (Figure 3). Therefore, the increase in measured decomposition enthalpies at higher pressures,

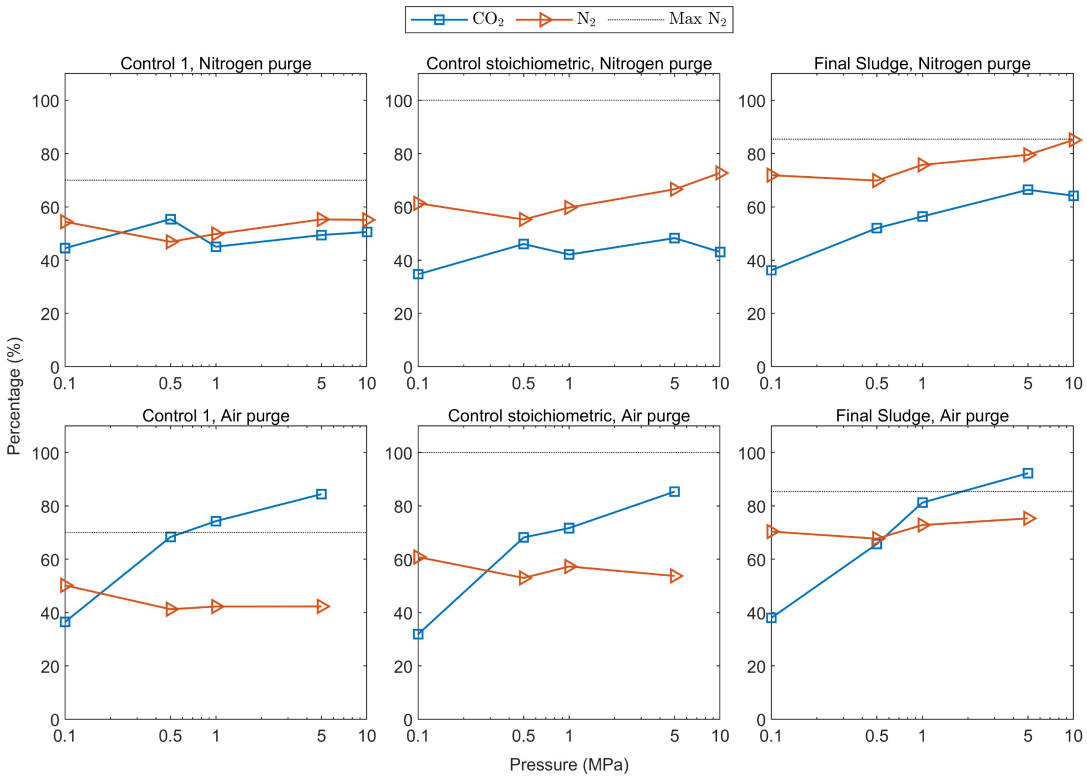

FIGURE 7 Mass percentages of sample carbon and nitrogen in CO_2 and N_2 respectively. Larger values signify higher extents of decomposition. Dotted lines show maximum theoretical N_2 yield from each sample.

as seen in Figure 3, is due in part by the reduction in the loss of sensible heat with hot gases. Further evidence of this phenomenon can be observed in the thermograms of the control and final sludge samples shown in Figure 8. Exothermic effects are shown with positive heat flow values, and only the regions between 100 °C and 370 °C are shown. The thermograms of the control samples at 0.1 MPa show an endothermic peak at around 300 °C, immediately before the exotherm. This endotherm is consistent with the endothermic effect of a sudden loss of gaseous species from the crucible [28]. This observation, and a comparison of the emissions and decomposition enthalpies from the control samples, lead to the conclusion that measured energy releases from the control samples are more significantly affected by the loss of sensible heat with the gaseous products at 0.1 MPa than at higher pressures.

The decomposition of the ANSol mixtures studied in this work was found to be strongly dependent on the sample composition and pressure at which the experiments were carried out. The decomposition temperatures for each sample were identified from the thermograms in Figure 8. For the FS samples, the decomposition temperature was determined as the onset temperature (T_{onset}) of the first exothermic peak, as determined by the STARe software. The decomposition temperature of the control samples was determined as the temperature where the thermogram deviated from the baseline after the endotherm of water vaporization.

For all cases, the decomposition temperature corresponds to the temperature at which the MANs decompose. The decomposition of MAN is reported to begin between 250 to 252 °C [20, 21], and the decomposition of the control samples begin between 260 and 270 °C, albeit at a slow rate. The decomposition temperatures of DMAN and TMAN at 0.1 MPa have been reported to be 203 °C and 186 °C, respectively [20], and the onset of the first exothermic peak of FS at this pressure is 220 °C. This exothermic peak is observed immediately after the endotherm of water vaporization. It is also noted that thermograms of the FS sample at different pressures show that the boiling point of water at a particular pressure is higher than normal due to the presence of hygroscopic species such as AN and MAN.

The contribution of the explosives (RDX and HMX) in the thermal decomposition of the FS sample can be distinguished in the FS thermograms at 0.1 MPa. Pure RDX and HMX have decomposition temperatures of 240 °C and 290 °C, respectively. However, both can undergo exothermic decomposition at lower temperatures with suitable additives [29, 30]. The inflection of the 0.1 MPa FS thermograms toward the exothermic direction at around 240 °C could be due to the decomposition of the RDX. Similarly, HMX decomposition could have

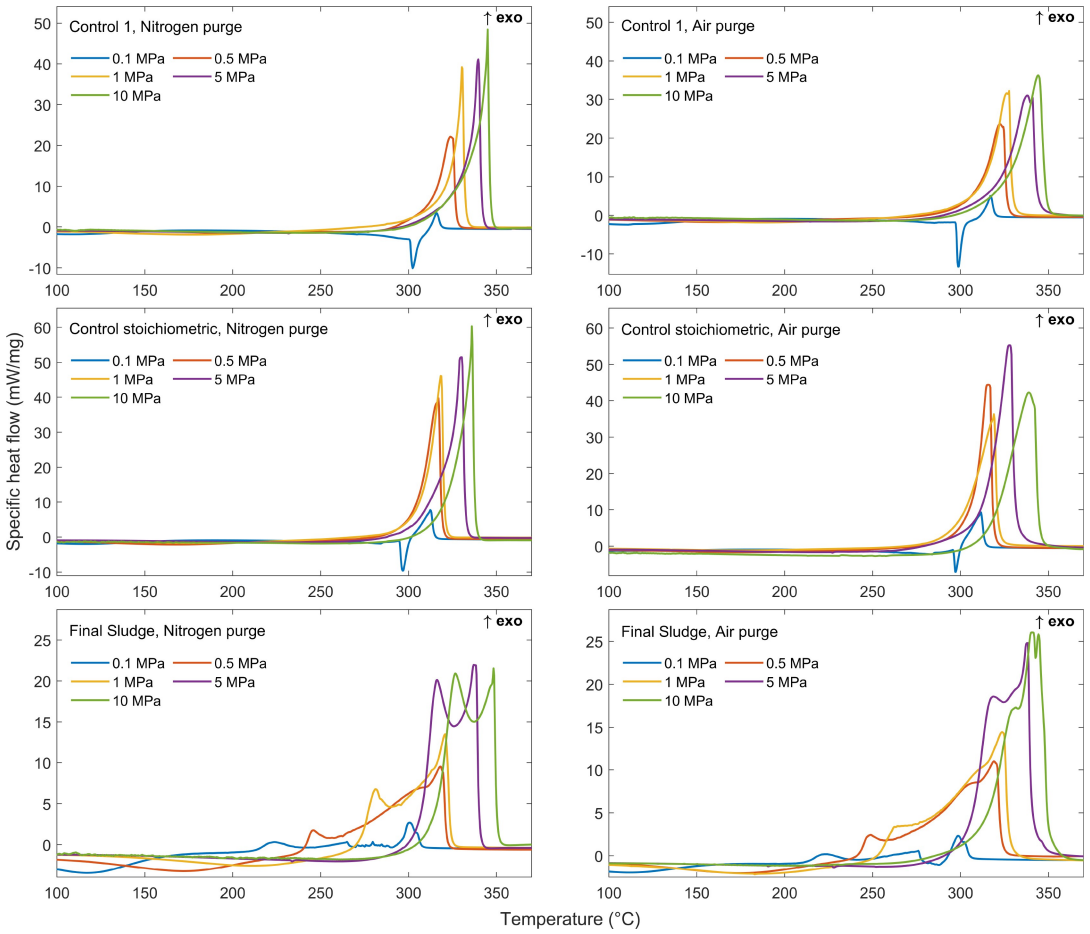

FIGURE 8 DSC thermograms of the control and final sludge samples at different pressures with N_2 and air purges. Exotherms of the final sludge sample appear earlier due to the presence of more reactive DMA and TMA.

contributed to the distinct exothermic peak of the FS sample near 300 °C at 0.1 MPa, which occurs at a slightly lower temperature than in the control samples. At higher pressures, the contributions of the DMAN, TMAN, and explosives are indistinguishable.

The onset of the first exothermic peak from the FS sample is shifted to higher temperatures as the pressure is increased. However, this exothermic peak is observed immediately after the endotherm of water vaporization, suggesting that water in the FS inhibits its exothermic decomposition. This phenomenon is attributed to the inhibition of HNO_3 dissociation according to reaction 3 [1, 8]. The ionic species from HNO_3 dissociation act as oxidizers for the carbon in the sample [7], and its inhibition also suppresses the decomposition of the sample. However, this effect fades away at high pressures. At 10 MPa, the normal boiling point of water is 311 °C; the effective boiling point of water in the sample is still higher. However, exothermic decomposition of the FS sample at 10 MPa begins at around 290 °C. The work of Brower et al. [9] demonstrated that above 290 °C, HNO_3 primarily decomposes via the radical mechanism discussed earlier (reaction 6), and that water does not inhibit this decomposition. Therefore, highly reactive radical oxidizing species are produced above this temperature regardless of the presence of water, and all samples decompose with significant heat flow rates.

The activation energies of the ionic and radical mechanisms of HNO_3 decomposition (reactions 3 and 6 respectively) are 89.9 kJ/mol and 181.6 kJ/mol respectively [31]. The radical mechanism is therefore activated at higher temperatures due to its higher activation energy. However, a comparison of the equilibrium and forward rate constants of these mechanisms, calculated using formulations and kinetic parameter values provided in [31–35] did not conclusively prove that the radical mechanism is kinetically favored after 290 °C. The pressure effects on these rates were also considered by employing formulations provided in [36, 37].

At lower pressures, FS samples have exothermic peaks at lower temperatures than the control samples, primarily due to the presence of DMAN, TMAN, and explosives (RDX and HMX). DMAN and TMAN decompose to produce dimethylamine [DMA, $(CH_3)_2NH$] and

trimethylamine [TMA, $(CH_3)_3N$] respectively, in addition to HNO_3 [20, 21]. Compared to the methylamine (MA) from MAN, the DMA and TMA have higher reactivities to oxidizing species [20], likely due to their lower bond dissociation energies [26, 38, 39]. As a result, the dissociation products of DMA and TMA react with the oxidizing species from HNO_3 dissociation (NO_2^+ and NO_3^-) producing the lower temperature exotherms. For the control samples, exothermic reactions proceed at a slow pace at lower temperatures due to comparatively lower reactivities of the MA from MAN, and NO_2^+ and NO_3^- from HNO_3. At temperatures above 290 °C, reactions proceed at a much faster rate, as evident by high heat flow rates, due to exothermic reactions between MA and the highly reactive $HO^\bullet$ and $NO_2^\bullet$ radicals.

5 | CONCLUSION

The thermal decomposition of the munitions wastewater (FS) and control samples (C1 and CS) at various pressures were studied, and the energy release and gaseous emissions produced were used as metrics to evaluate the decomposition. Experimental results showed that higher pressures improved the decomposition enthalpies and reduced the quantities of harmful NO_x from all samples. Under nitrogen pressure, the maximum energy releases from the C1, CS, and FS samples were 1.7 MJ/kg, 1.9 MJ/kg, and 1.8 MJ/kg respectively at 10 MPa; this level of energy release is approximately 45% of the upper bound estimated by the standard enthalpy of decomposition. It is likely that an appreciable portion of this deficit is due to sensible heat and gaseous intermediates leaving the pin-hole crucible prior to being accounted for by the DSC. The pin-hole crucibles were used in the DSC because emissions measurement was a first-order requirement for this study.

The major gaseous species in the emissions stream from the decomposition of the samples were CO_2, N_2O and N_2 (obtained from nitrogen mass balance). The minor gaseous species were CO, NO and NO_2. The amounts of all nitrogen oxides decreased with pressure, and NO and NO_2 were found in minuscule quantities at 10 MPa. For the decomposition of the FS sample at 10 MPa, only 0.7% of the nitrogen in the sample was found in NO, and 0.08% in NO_2.

At lower pressures, the decomposition of the final sludge sample proceeded via reactions between oxidizing species from HNO_3 dissociation and DMA and TMA from the dissociation of DMAN and TMAN, respectively. However, the decomposition of the control samples proceeded at an appreciable rate only after 290 °C. This phenomenon was ascribed to the relatively low reactivity of the ionic oxidizing species of HNO_3 dissociation and of MA from MAN dissociation. After 290 °C, HNO_3 decomposed via a radical mechanism to produce highly reactive radical species, which promptly reacted with the methyl groups of the MA. In higher pressure experiments, the presence of water inhibited the ionic decomposition of HNO_3, and the decomposition of all samples was driven by the radical products of HNO_3 above 290 °C.

Experimental results from this work have demonstrated that the thermal decomposition of the final sludge is a net energy positive process, with minimum amounts of harmful emissions, particularly NO_x. These results, however, have been affected by the loss of sensible heat and reactants from the pin-hole crucibles in the DSC. It is therefore concluded that an appropriately designed system can further improve the energy and emissions yields from the munitions wastewater.

CONFLICT OF INTEREST STATEMENT

The authors have no conflict of interest.

DATA AVAILABILITY STATEMENT

Data will be made available upon reasonable request.

ORCID

Roshan Adhikari http://orcid.org/0000-0002-7065-6422
Nick Parziale http://orcid.org/0000-0001-9880-1727

REFERENCES

1. S. Chaturvedi, P. N. Dave, *J. Energ. Mater.* **2013**, *31*, 1–26, 10.1080/07370652.2011.573523.
2. C. J. Oommen, S. R. Jain, *J. Hazard. Mater.* **1999**, *67*, 253–281, 10.1016/S0304-3894(99)00039-4.
3. V. P. Sinditskii, V. Y. Egorshev, A. I. Levshenkov, V. V. Serushkin, *Propellants Explos. Pyrotech.* **2005**, *30*, 269–280, 10.1002/prep.200500017.
4. M. Negovanović, L. Kričak, S. Milanović, N. Đokić, N. Simić, *Podzemni radovi* **2015**, *27*, 49–63, 10.5937/podrad1527049N.
5. A. G. Dana, G. Tvil, L. Winter, G. E. Shter, G. S. Grader, *Fuel* **2015**, *159*, 500–507, 10.1016/j.fuel.2015.06.099.
6. G. Feick, R. Hainer, *J. Am. Chem. Soc.* **1954**, *76*, 5860–5863, 10.1021/ja01651a096.
7. Y.-I Izato, A. Miyake, S. Date, *Propellants Explos. Pyrotech.* **2013**, *38*, 129–135, 10.1002/prep.201100106.
8. W. A. Rosser, S. H. Inami, H. Wise, *J. Phys. Chem.* **1963**, *67*, 1753–1757, 10.1021/j100803a004.
9. K. R. Brower, J. C. Oxley, M. Tewari, *J. Phys. Chem.* **1989**, *93*, 4029–4033, 10.1021/j100347a033.
10. V. Babrauskas, D. Leggett, *Fire Mater.* **2020**, *44*, 250–268, 10.1002/fam.2797.
11. B. A. Lurie, C. Lianshen, *Combust. Explos. Shock Waves* **2000**, *36*, 607–617, 10.1007/BF02699524.

12. Z.-X. Xu, Q. Wang, X. Zhu, X.-Q. Fu, *J. Therm. Anal. Calorim.* **2017**, *130*, 1171–1179, 10.1007/s10973-0176486-y.
13. R. G. Parker, *J. Forensic Sci.* **1975**, *20*, 257–260, 10.1520/JFS10272J.
14. A. G. Dana, G. E. Shter, G. S. Grader, *RSC Adv.* **2014**, *4*, 10051–10059, 10.1039/c3ra47890d.
15. A. G. Dana, B. Mosevitzky, G. Tvil, M. Epstein, G. E. Shter, G. S. Grader, *Energy Fuels* **2016**, *30*, 2474–2477, 10.1021/acs.energyfuels.6b00115.
16. A. G. Dana, G. E. Shter, G. S. Grader, *RSC Adv.* **2014**, *4*, 34836–34848, 10.1039/C4RA04381B.
17. B. Mosevitzky, A. G. Dana, G. E. Shter, G. S. Grader, *Combust. Flame* **2016**, *166*, 295–306, 10.1016/j.combustflame.2016.01.030.
18. W.-M Chien, D. Chandra, K. H. Lau, D. L. Hildenbrand, A. M. Helmy, *J. Chem. Thermodyn.* **2010**, *42*, 846–851, 10.1016/j.jct.2010.01.012.
19. T. P. Russell, T. B. Brill, *Combust. Flame* **1989**, *76*, 393–401, 10.1016/0010-2180(89)90120-X.
20. S. R. Jain, M. V. Rao, V. R. Pai Verneker, *Propellants Explos. Pyrotech.* **1978**, *3*, 83–87, 10.1002/prep.19780030302.
21. Y. Miron, *J. Hazard. Mater.* **1980**, *3*, 301–321, 10.1016/0304-3894(80)80003-3.
22. C. A. R. Pappijn, F. H. Vermeire, R. Van de Vijver, M.-F Reyniers, G. B. Marin, K. M. Van Geem, *Proc. Combust. Inst.* **2021**, *38*, 585–592, 10.1016/j.proci.2020.07.045.
23. S.-D. Clas, C. R. Dalton, B. C. Hancock, *Pharm. Sci. Technol. Today* **1999**, *2*, 311–320, 10.1016/S1461-5347(99)00181-9.
24. E. García, D. Sánchez-Rodríguez, J. P. López-Olmedo, J. Farjas, P. Roura, *J. Therm. Anal. Calorim.* **2015**, *121*, 187–194, 10.1007/s10973-015-4465-8.
25. Q. Chen, R. Yang, B. Zhao, Y. Li, S. Wang, H. Wu, Y. Zhuo, C. Chen, *Fuel* **2014**, *134*, 467–476, 10.1016/j.fuel.2014.05.092.
26. D. G. Patil, S. R. Jain, T. B. Brill, *Propellants Explos. Pyrotech.* **1992**, *17*, 99–105, 10.1002/prep.19920170302.
27. H. Muckenhuber, H. Grothe, *Carbon* **2006**, *44*, 546–559, 10.1016/j.carbon.2005.08.003.
28. S. P. Green, K. M. Wheelhouse, A. D. Payne, J. P. Hallett, P. W. Miller, J. A. Bull, *Angew. Chem.* **2020**, *132*, 15930–15934, 10.1002/ange.202007028.
29. G. Hussain, G. J. Rees, *Fuel* **1995**, *74*, 273–277, 10.1016/0016-2361(95)92665-S.
30. G Hussain, G. J. Rees, *Propellants Explos. Pyrotech.* **1995**, *20*, 74–78, 10.1002/prep.19950200206.
31. Y.-I. Izato, A. Miyake, *J. Therm. Anal. Calorim.* **2018**, *134*, 813–823, 10.1007/s10973-018-7322-8.
32. G. Schott, N. Davidson, *J. Am. Chem. Soc.* **1958**, *80*, 1841–1853, 10.1021/ja01541a019.
33. G. D. Robertson Jr, D. M. Mason, W. H. Corcoran, *J. Phys. Chem.* **1955**, *59*, 683–690, 10.1021/j150530a004.
34. C. A. Cantrell, J. A. Davidson, A. H. McDaniel, R. E. Shetter, J. G. Calvertv, *J. Chem. Phys.* **1988**, *88*, 4997–5006, 10.1063/1.454679.
35. R. S. Zhu, M. Lin, *J. Chem. Phys.* **2003**, *119*, 10667–10677, 10.1016/S0009-2614(02)00063-5.
36. V. L Stanford, T. Liavitskaya, S. Vyazovkin, *J. Phys. Chem. C* **2019**, *123*, 21059–21065, 10.1021/acs.jpcc.9b06272.
37. S. Vyazovkin, *Int. Rev. Phys. Chem.* **2020**, *39*, 35–66, 10.1080/0144235X.2019.1691319.
38. T. J. Burkey, A. L. Castelhano, D. Griller, F. P. Lossing, *α-Aminoalkyl radicals. J. Am. Chem. Soc.* **1983**, *105*, 4701–4703, 10.1021/ja00352a029.
39. D. D. M. Wayner, K. B. Clark, A. Rauk, D. Yu, D. A. Armstrong, *Journal of the American Chemical Society* **1997**, *119*, 8925–8932, 10.1021/ja971365v.

How to cite this article: R. Adhikari, N. Parziale, T.-L. Su, W. Braida, C. Christodoulatos, *Propellants, Explos., Pyrotech.* **2024**, *49*, e202300139. https://doi.org/10.1002/prep.202300139